ACS Catalysis

pubs.acs.org/acscatalysis Research Article

Role of Ligand-Bound CO_2 in the Hydrogenation of CO_2 to Formate with a (PNP)Mn Catalyst

Kevin Schlenker, Elizabeth G. Christensen, Asylbek A. Zhanserkeev, Gabriel R. McDonald, Emily L. Yang, Kevin T. Lutz, Ryan P. Steele, Ryan T. VanderLinden, and Caroline T. Saouma*

Cite This: *ACS Catal.* 2021, 11, 8358–8369 Read Online

ACCESS | Metrics & More | Article Recommendations | Supporting Information

ABSTRACT: Herein, we describe the catalytic hydrogenation of CO_2 to formate with **(PNP)Mn−H** (PNP = 2,6-bis(di-*tert*-butylphosphinomethyl)-pyridine; Mn = $Mn(CO)_2$). Contrary to the established mechanism for CO_2 hydrogenation, mechanistic studies indicate that CO_2 does not insert into the Mn−H bond of **(PNP)Mn−H** to give the formate species, **(PNP)Mn−OCHO**. The lack of reactivity is confirmed by thermochemical studies that show that **(PNP)Mn−H** is not sufficiently hydridic to reduce CO_2. Deprotonation of the hydride to give $[(^*\mathbf{PNP})\mathbf{Mn{-}H}]^-$ (* indicates the deprotonated ligand) enhances the hydricity by ∼17 kcal·mol^{-1} and hence should be sufficiently hydridic to hydrogenate CO_2. This reactivity is not observed, and CO_2 instead binds to the backbone to generate another anionic hydride species $[(\mathbf{CO_2\text{-}PNP})\mathbf{Mn{-}H}]$. The formate is lost only from this species, through hydride transfer to an external CO_2. These findings are unexpected because substrate binding to the backbone of catalysts that can undergo metal−ligand cooperativity (MLC) is thought to be detrimental to catalysis; this work suggests that alternative mechanisms should be considered. The enhanced hydricity observed upon deprotonation may be broadly applicable to systems capable of undergoing MLC. Moreover, this work shows an example of how thermochemical analysis can be used to advance mechanistic understanding in (de)hydrogenation catalysis.

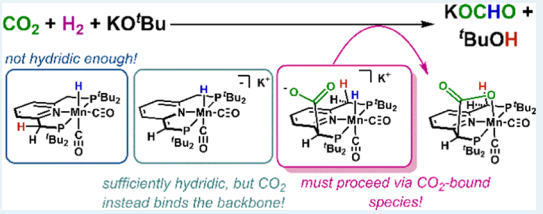

KEYWORDS: *CO_2 hydrogenation, catalysis, metal−ligand cooperativity, mechanisms, thermodynamic parameters*

INTRODUCTION

Advancing the hydrogenation of CO_2 to formate or formic acid (FA) is motivated by increased global energy demands.[1−3] Formic acid is primarily produced from CO on a 720 000 t annual scale,[4] and the development of formic acid fuel cells,[5] using FA as a H_2 carrier,[6] and further hydrogenation to MeOH[1] will only increase demand. Despite numerous examples of homogeneous catalysts that hydrogenate CO_2 to FA, better catalysts should be developed that allow for high turnover numbers (TONs) and frequencies (TOFs) under mild conditions.[1]

The CO_2 insertion into a M−H to give M−OCHO is thought to be a critical step in the mechanism of converting CO_2 to formate or FA.[7−10] Insight into this process has been gleaned from kinetic studies that explore how solvent, Lewis acids, and ligands impact the rate of CO_2 insertion,[11,12] as well as thermodynamic analysis of intermediate metal hydrides.[13−17]

The insertion of CO_2 into the M−H is also pertinent for catalysts that are capable of undergoing metal−ligand cooperativity (MLC). Pincer-ligated Ru,[14,18−20] Co,[21,22] Fe,[23−25] and Mn[26,27] complexes have emerged as promising catalysts for the hydrogenation of CO_2 to formate, with some Ru catalysts capable of converting CO_2 to MeOH[14,19,28,29] in the presence of amines. A proposed mechanism is shown in Scheme 1 (left) for the hydrogenation of CO_2 to formate that makes use of MLC.[18] The dearomatized (or deprotonated) catalyst heterolytically adds H_2, with ligand protonation concomitant to formation of the metal hydride. CO_2 then inserts into the metal hydride to give a formate-bound species. The base-mediated formate loss ensues via ligand deprotonation to regenerate the dearomatized (or deprotonated) species. Alternative mechanisms that do not rely on MLC have also been proposed,[30,31] as indicated by the dashed arrows in Scheme 1.

An underexplored pathway for CO_2 hydrogenation involves activation of CO_2 through MLC to generate a $(CO_2{-}L)M$ adduct. In this reaction, the Lewis-basic ligand attacks the Lewis-acidic carbon of CO_2 to give a ligand-bound species and one oxygen of the bound CO_2 coordinates the metal, giving the metal an electron count of 18 (Scheme 1, right). Ru,[14,18,32,33] Mn,[27] and other metals[25,34−36] have been shown to activate CO_2 in this manner. Moreover, other hydrogenation substrates can coordinate to catalysts capable of MLC

Received: April 14, 2021
Revised: June 5, 2021
Published: June 23, 2021

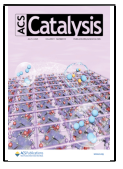

https://doi.org/10.1021/acscatal.1c01709
ACS Catal. 2021, 11, 8358–8369

Scheme 1. (Left): Proposed Mechanism for CO_2 Hydrogenation to Formate by (PNE)-Ligated Ru (E = P^tBu_2 or NEt_2) That Undergoes MLC (Black Arrows); the Alternative Direct (dashed) Pathway is also Shown. (Right): Ligand-Bound CO_2 is Thought to be Detrimental to Catalysis or to Engage in an Alternative, Minor Pathway

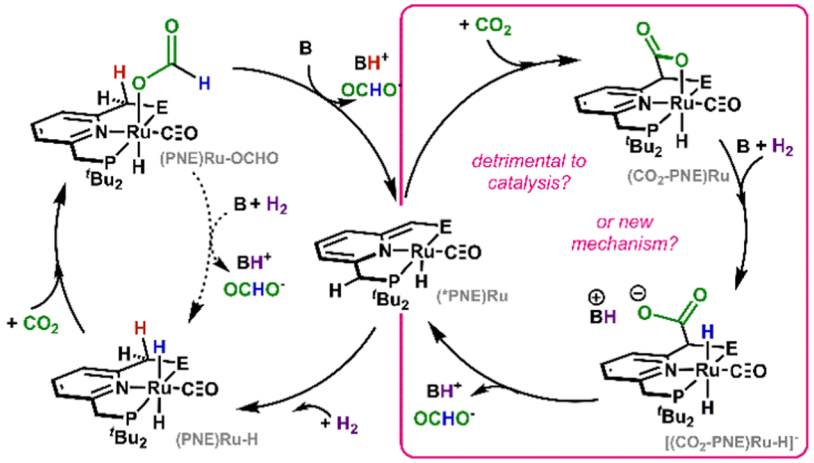

analogously,[37−39] suggesting that this reactivity may occur more broadly.

For CO_2 hydrogenation at Ru, mechanistic studies by Sanford suggest that a CO_2-bound species may hydrogenate CO_2 under an alternative mechanistic scheme (Scheme 1, right);[18] this pathway is thought to be minor relative to that shown on the left of Scheme 1. However, density functional theory (DFT) studies by Pidko on a related catalyst suggest that a pathway with a ligand-bound CO_2 is not favored,[40] and Milstein suggests that the analogous species on Fe is off-cycle.[25]

Given that binding of CO_2 is competitive to H_2 binding at Ru,[14] we sought to unequivocally establish if such complexes are pertinent to the hydrogenation of CO_2. Herein, we describe the catalytic hydrogenation of CO_2 to formate with a Mn catalyst. Mechanistic and thermochemical studies are not consistent with the established step of CO_2 inserting into a neutral metal hydride, akin to that shown on the left of Scheme 1. While thermodynamically favorable, hydrogenation of CO_2 to formate by an anionic Mn−H also does not occur. Rather, our studies suggest that formate is produced from an anionic Mn−H that has a ligand-bound CO_2, analogous to that shown in Scheme 1 (right). Compared to the prior work on Ru,[18] our studies suggest that formate loss occurs from the ligand-bound intermediate. Given the ability to deprotonate catalysts that undergo MLC, and the range of catalysts that react with the substrate via MLC at the backbone,[14,18,25,27,32−39] the results are broadly relevant to advancing (de)hydrogenation mechanisms at catalysts that can undergo MLC.

RESULTS AND DISCUSSION

Choice of the System. Given that Mn has been shown to hydrogenate[26,27,41] and electrocatalytically reduce CO_2 to formate,[16,42] as well as dehydrogenate formic acid to CO_2 and H_2,[43,44] we sought to explore the hydrogenation of CO_2 using **(PNP)Mn−H** (PNP = 2,6-bis(di-*tert*-butylphosphinomethyl)pyridine; Mn = $Mn(CO)_2$).[38] This ligand was chosen so that the thermochemical parameters can be compared to the Ru analogue, **(PNP)Ru(CO)H_2**,[14] which differs in metal identity and replacement of one CO with a hydride.

Catalytic Hydrogenation of CO_2. The hydrogenation of CO_2 in the presence of 100 equiv of KO^{t}Bu was examined using two Mn complexes, the putative active hydride, **(PNP)Mn−H**,[38] and the ligand-bound CO_2 species, **(CO_2-PNP)Mn**. This species is readily prepared by treatment of **(*PNP)Mn** with 0.85 atm.[45] of CO_2 (the dearomatized ligand is designated by *).

In the presence of 100 equiv of KO^{t}Bu, **(PNP)Mn−H** hydrogenates CO_2 to formate (Table 1, entries 1−4). With

Table 1. Hydrogenation of CO_2 by Mn Catalysts

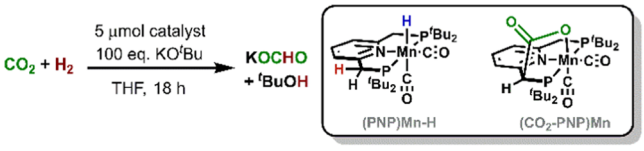

entry[a]	P_{CO_2} (bar)	P_{H_2} (bar)	T (°C)	catalyst	TON[b] formate
1	8	8	50	**(PNP)Mn−H**	9 (8)
2	8	8	100	**(PNP)Mn−H**	17 (6)
3	15	15	50	**(PNP)Mn−H**	5 (3)
4	15	15	100	**(PNP)Mn−H**	58 (15)
5[c]	15	15	100	**(PNP)Mn−H**	2 (1)
6	15	15	100	**(CO_2-PNP)Mn**	49 (15)
7	15	15	100	--	0
8	15	0	100	**(PNP)Mn−H**	0
9	0	15	100	**(PNP)Mn−H**	0

[a]Reactions were run in 10 mL of tetrahydrofuran (THF). [b]Quantified via ion chromatography, see the Supporting Information (SI). Average of 3 runs, with the standard deviation given in parentheses. [c]No base added.

equivalent pressures of CO_2 and H_2, the turnover number (TON) increases as the temperature is increased from 50 to 100 °C and with increasing the overall pressure of the gases. As shown in entry 5, addition of a base is required for the formation of formate (or FA).

Next, the catalytic activity of **(CO_2-PNP)Mn** was considered. Under identical conditions to **(PNP)Mn−H** (entries 4 vs 6), **(CO_2-PNP)Mn** gives the same TON within error. Omission of the catalyst, H_2, or CO_2 gives no formate (entries 7−9). The unoptimized catalytic trials clearly indicate that

https://doi.org/10.1021/acscatal.1c01709
ACS Catal. 2021, 11, 8358−8369

Scheme 2. Plausible Mechanisms Consistent With the Catalytic Hydrogenations

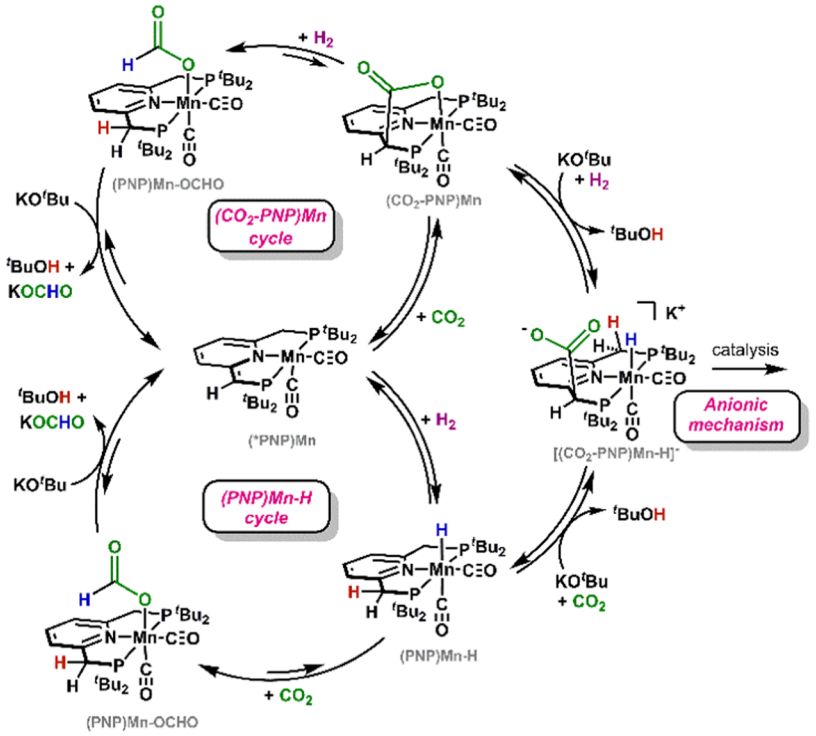

both **(CO$_2$-PNP)Mn** and **(PNP)Mn−H** can access a catalytic cycle.

Though ligand-bound CO$_2$ species have been invoked to be detrimental to catalysis,[25,40] these results are consistent with the following 3 scenarios. First, catalysis ensues through **(PNP)Mn−H** (Scheme 2, bottom), and **(CO$_2$-PNP)Mn** is off-cycle but can enter the cycle through loss of CO$_2$. This scenario is consistent with established mechanisms for CO$_2$ hydrogenation. Second, catalysis ensues through **(CO$_2$-PNP)Mn** (Scheme 2, top) and **(PNP)Mn−H** is off-cycle but can enter through the loss of H$_2$. Such a mechanism has no literature precedence and is included for completeness. Third, both **(CO$_2$-PNP)Mn** and **(PNP)Mn−H** can be transformed to a catalytically viable intermediate (Scheme 2, right). Given that catalysis proceeds under basic conditions and prior work on Ru,[18] **[(CO$_2$-PNP)Mn−H]$^-$** is considered a plausible intermediate that is accessible from both **(CO$_2$-PNP)Mn** and **(PNP)Mn−H** (Scheme 2, right). All three scenarios invoke MLC at the ligand.

Stoichiometric Reactions Pertinent to Formate Production via (PNP)Mn−H. To determine if the cycle that proceeds through **(PNP)Mn−H** is correct (Scheme 2, bottom), stoichiometric studies were conducted to determine feasibility. Independent synthesis of **(PNP)Mn−OCHO** was undertaken to identify its formation and reactivity toward the base. Treatment of equimolar **(*PNP)Mn** and formic acid in pentanes results in the precipitation of a yellow powder. The solid has an IR stretch at 1625 cm^{-1}, and the ^{1}H NMR spectrum has a resonance at 8.47 ppm, both consistent with a formate species. A single resonance at 105.9 ppm is observed in the ^{31}P NMR spectrum. Taken together, this is consistent with the product being **(PNP)Mn−OCHO**.

Unlike the Ru analogue, **(PNP)Ru(CO)(H)(OCHO)**,[14] THF solutions of **(PNP)Mn−OCHO** are not stable; over the course of hours, conversion to **(PNP)Mn−H** occurs with loss of the free ligand (Scheme 3). Attempts to stabilize **(PNP)Mn−OCHO** by placement under a CO$_2$ atmosphere

Scheme 3. (Top): Stability of (PNP)Mn−OCHO in THF. (Bottom): Reactivity of (PNP)Mn−OCHO toward the Base

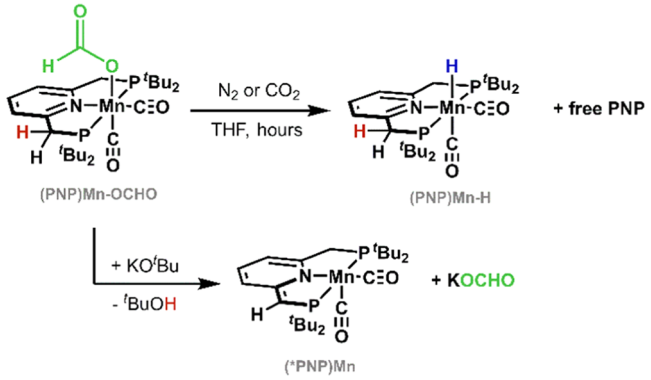

were not successful (see Figure S19). This suggests that the observed reactivity is not simply a deinsertion of CO$_2$; the product **(PNP)Mn−H** is stable under N$_2$ and CO$_2$.

To determine if CO$_2$ inserts into the Mn−H bond to give a formate species, a THF solution of **(PNP)Mn−H** was placed under 0.85 atm of CO$_2$.[45] As ascertained by ^{31}P NMR spectroscopy, no reaction occurred. When the reaction was repeated using 30 bar of CO$_2$ at 50 °C, the only species present upon cooling and replacing under a N$_2$ atmosphere was **(CO$_2$-PNP)Mn** (Scheme 4).

It is conceivable that small amounts of **(PNP)Mn−OCHO** form in the equilibrium of **(PNP)Mn−H** with CO$_2$, and that deprotonation of **(PNP)Mn−OCHO** produces formate and **(*PNP)Mn** (Scheme 2, bottom cycle). Indeed, treatment of **(PNP)Mn−OCHO** with 1 equiv of KO^{t}Bu rapidly produces **(*PNP)Mn** and KOCHO (Scheme 3). If this mechanism is

https://doi.org/10.1021/acscatal.1c01709
ACS Catal. 2021, 11, 8358−8369

Scheme 4. Stoichiometric Reactions Pertinent to the (PNP)Mn−H Cycle

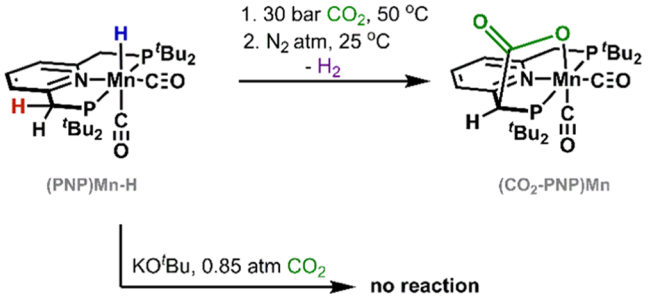

correct, then treatment of **(PNP)Mn−H** with 1 equiv of KO^{t}Bu at 0.85 atm of CO_2 should result in formate loss and the formation of **(*PNP)Mn** (Scheme 4); no reaction is observed (Figure S48). Taken together, this suggests that the mechanism that proceeds via neutral **(PNP)Mn−H** is not operational under the mild conditions investigated. These conditions differ from those of Table 1, where the elevated temperature may allow for kinetic barriers to be overcome and/or for different thermodynamics parameters to be present,[17] while the elevated pressures may shift equilibria between the catalyst and gaseous substrates.

Stoichiometric Reactions Pertinent to Formate Production via (CO$_2$-PNP)Mn. Though there is no precedence for H_2 "insertion" into species akin to **(CO$_2$-PNP)Mn**, it is considered as a mechanistic possibility (Scheme 2, top). Under ambient conditions (0.85 atm H_2, 20 °C), no reaction occurs between **(CO$_2$-PNP)Mn** and H_2. After exposure to 30 bar of H_2 and 50 °C, the major species in solution upon returning to ambient conditions is **(PNP)Mn−H**, with ∼13% of the desired **(PNP)Mn−OCHO** (Scheme 5).

Treatment of **(CO$_2$-PNP)Mn** with 1 equiv of KO^{t}Bu and 0.85 atm H_2 results in formate loss and the formation of **(PNP)Mn−H** (Scheme 5). This is consistent with the mechanism shown in the top of Scheme 2, provided that once **(*PNP)Mn** is formed it reacts with H_2 to generate **(PNP)Mn−H** and enters the bottom cycle (reversibly). However, **(CO$_2$-PNP)Mn** is readily deprotonated with 1 equiv of KO^{t}Bu to give **[(*CO$_2$-PNP)Mn]$^-$** (Scheme 5). The anionic species further reacts with H_2 to give **[(CO$_2$-PNP)Mn−H]$^-$** (shown in Scheme 2, right, and vide infra), whereas neutral **(CO$_2$-PNP)Mn** requires elevated pressures of H_2 to give **(PNP)Mn−H** and **(PNP)Mn−OCHO** (vide supra). These results are not consistent with the mechanism shown at the top of Scheme 2 under ambient conditions. Taken together, the mechanistic studies suggest that a mechanism that proceeds via neutral **(CO$_2$-PNP)Mn** (with no deprotonation, top of Scheme 2) is not viable under mild conditions.

Thermochemical Analysis Pertinent to Catalysis via Neutral Cycles. To better understand the observed reactivity that is pertinent to the mechanisms of Scheme 2, the equilibria shown in Scheme 6 were measured or extrapolated. These measurements were all done in THF, to best describe their values under catalytic conditions. The equilibrium of **(*PNP)Mn** with H_2 or CO_2 to give **(PNP)Mn−H** or **(CO$_2$-PNP)Mn**, respectively (K_1 or K_2), was monitored by UV−vis spectroscopy. To observe equilibrium mixtures, very low pressures of either gas had to be introduced via a calibrated bulb (see the SI), and the solution allowed to equilibrate.

As shown in Table 2, the binding of H_2 (−3.3 kcal·mol^{-1}) and CO_2 (−3.7 kcal·mol^{-1}) is favorable under standard conditions. These values are comparable to those obtained for **(*PNP)Ru(CO)(H)**, whereby similar energies are associated with both H_2 (−4.1 kcal·mol^{-1}) and CO_2 (−3.8 kcal·mol^{-1}).[14] Under 30 bar of gas, the free energies for both equilibria decrease by 2 kcal·mol^{-1}, further stabilizing **(PNP)-Mn−H** and **(CO$_2$-PNP)Mn** relative to **(*PNP)Mn**.

The equilibrium of **(*PNP)Mn** with FA to give **(PNP)Mn−OCHO** (K_3, ΔG_{FA}) was monitored by ^{31}P NMR spectroscopy

Scheme 5. Stoichiometric Reactions Pertinent to the (CO$_2$-PNP)Mn Cycle

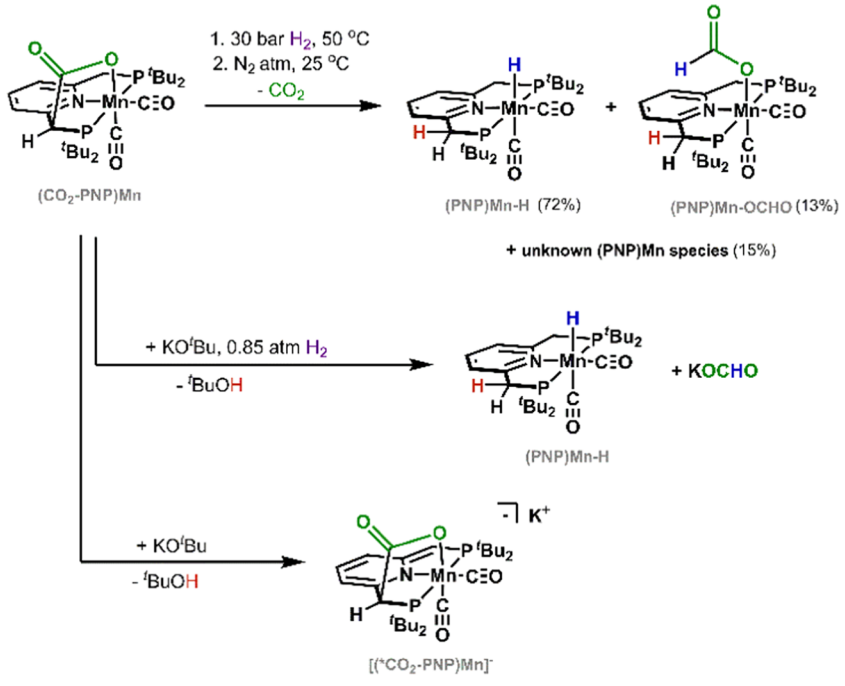

https://doi.org/10.1021/acscatal.1c01709
ACS Catal. 2021, 11, 8358−8369

Scheme 6. Equilibrium Constants and Thermodynamic Parameters Measured (K_1, K_2, K_3, K_4, K_{11}) and Extrapolated (K_5, K_6, K_{12}) in THF

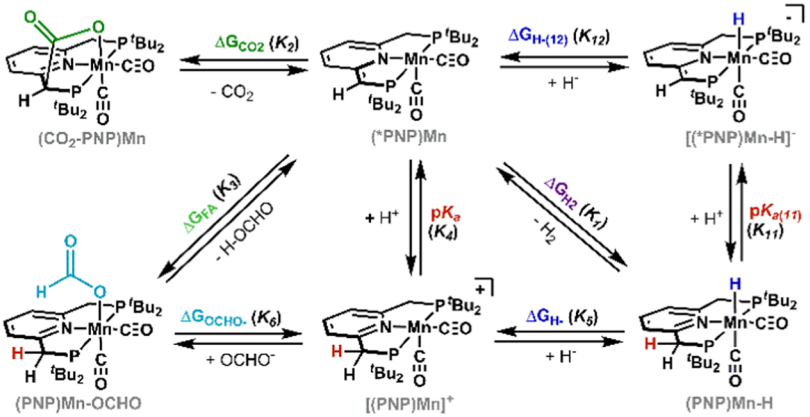

Table 2. Equilibrium Constants and Free-Energy Changes Associated With the Equilibria of Scheme 6

[a]equilibrium	[d]K	$\Delta G°$ (kcal·mol^{-1})	[e]ΔG (30 bar)
[b]K_1 (ΔG_{H_2})	280 ± 10	−3.3 ± 0.2	−5.3
[b]K_2 (ΔG_{CO_2})	480 ± 10	−3.7 ± 0.2	−5.7
[b]K_3 (ΔG_{FA})	∼1100	∼−4.1	
[c]K_4 (ΔG_4)	1.6×10^{-19}	25.6 ± 0.3	
[c]K_5 (ΔG_{H^-})	9.8×10^{-35}	46.4 ± 0.4	
[c]K_6 (ΔG_{OCHO^-})	$\sim 9.1 \times 10^{-6}$	∼6.9	
[c]K_{11} (ΔG_{11})	6.3×10^{-32}	42.5 ± 0.3	
[c]K_{12} ($\Delta G_{H^-(anion)}$)	2.5×10^{-22}	29.5 ± 0.3	

[a]All measurements were done at 25 °C. [b]Units in M^{-1}. [c]Units in M. [d]Under standard conditions. [e]Conversion to nonstandard conditions: $\Delta G_x = \Delta G_x° - RT\ln(Y)$ where Y is the partial pressure of gas.[14] Units in kcal·mol^{-1}.

(Scheme 6, top-middle to bottom-left). This approach allows for quantification of **(PNP)Mn−H** and other degradation products that arise from the instability of **(PNP)Mn−OCHO** (Scheme 3). Because the reaction of **(*PNP)Mn** with FA is fast to equilibrate and the subsequent reactivity is slow, the value obtained is assumed to be ∼ representative of K_3 and found to be ∼1100 M^{-1} under standard conditions (see the SI for details). Hence, **(PNP)Mn−OCHO** is favored over **(*PNP)Mn** by ∼4.1 kcal·mol^{-1} with 1 M FA. The analogous equilibrium on Ru[14] is favored by 3.5 kcal·mol^{-1} under standard conditions. Despite the equilibrium to yield **(PNP)Mn−OCHO** being more favorable than on Ru, degradation is only observed from **(PNP)Mn−OCHO**.

To determine if hydride transfer from **(PNP)Mn−H** to CO_2 is thermodynamically favorable, the hydricity of **(PNP)Mn−H** must be determined. This is done following the thermochemical cycle in Scheme 7, whereby the first two equations correspond to equilibria that are pictorially shown in Scheme 6.

Titration of **[(PNP)Mn]$^+$** with various equivalents of the phosphazene base, $(OMeC_5H_4N)P(pyrr)_3$, (pK_{ip} = 16.8),[47] gives a pK_{ip} value of 18.8 ± 0.2 for **[(PNP)Mn]$^+$**. The cation is more acidic than **[(PNP)Ru(CO)H]$^+$**, which has a pK_{ip} of 20.7 ± 0.2.[14] The increased acidity on Mn suggests that the anionic charge on the ligand is better stabilized, likely through enhanced π-backbonding interactions relative to the Ru analogue.

Scheme 7. Equilibria Employed to Determine the Hydricity[a]

$(PNP)Mn-H \rightleftharpoons (^*PNP)Mn + H_2$	$-\Delta G_{H2} = 3.3$	$(K_1)^{-1}$
$(^*PNP)Mn + H^+ \rightleftharpoons [(PNP)Mn]^+$	$-\Delta G_4 = -25.6$	$(K_4)^{-1}$
$H_2 \rightleftharpoons H^+ + H^-$	$\Delta G_7 = 68.7$	K_7
$(PNP)Mn-H \rightleftharpoons [(PNP)Mn]^+ + H^-$	$\Delta G_{H^-} = 46.4$	K_5

[a]Free energies are in units of kcal·mol^{-1}. The value of ΔG_7 is from ref 46.

From the sum of equations shown in Scheme 7, the hydricity of **(PNP)Mn−H** in THF is found to be 46.4 kcal·mol^{-1}. Compared to **(PNP)Ru(CO)(H)$_2$**, the Mn hydride is 1.8 kcal·mol^{-1} less hydridic (higher ΔG_{H^-} value). This difference in hydricity has also been corroborated by direct equilibrium measurements made between the Mn and Ru systems (see Figure S43).

The lack of reactivity between **(PNP)Mn−H** and CO_2 to give formate and **[(PNP)Mn]$^+$** indicates that **(PNP)Mn−H** is less hydridic than formate. While the hydricity of formate is not known in THF, we previously reported a lower limit of 44.7 kcal·mol^{-1}.[14] Hence, direct hydride transfer from **(PNP)Mn−H** to CO_2 is <1.7 kcal·mol^{-1} uphill.

The above analysis assumes that the resulting formate does not bind to the metal. As shown by Miller[48] and us,[14] the effective hydricity can be increased by binding of an anion to the resulting cation, in this case, formate binding yields **(PNP)Mn−OCHO**. Hence, the effective hydricity is the sum of the hydricity of the hydride, in this case **(PNP)Mn−H**, and the energy associated with binding the anion to the cation, in this case formate binding to **[(PNP)Mn]$^+$** (sum of vertical equilibria in Scheme 8).

To determine the effective hydricity upon formate binding, the energy associated with formate release from **(PNP)Mn−OCHO** to give **[(PNP)Mn]$^+$** must be known (ΔG_{OCHO^-}, K_6). From the equations of Scheme 9, the binding of formate to the cation ($-\Delta G_{OCHO^-}$) is favorable by ∼6.9 kcal·mol^{-1}; this value compares well to that at other Mn(I) complexes.[16] Hence, the effective hydricity (Scheme 8) is ∼39.5 kcal·mol^{-1}. If the effective hydricity is greater than the hydricity of formate, then CO_2 insertion into **(PNP)Mn−H** to give **(PNP)Mn−OCHO** ($(K_{10})^{-1}$) is thermodynamically favorable. This analysis shows that by accounting for formate coordination, the reaction with

https://doi.org/10.1021/acscatal.1c01709
ACS Catal. 2021, 11, 8358−8369

Scheme 8. Equilibria Pertinent to CO_2 Deinsertion and the Effective Hydricity[a]

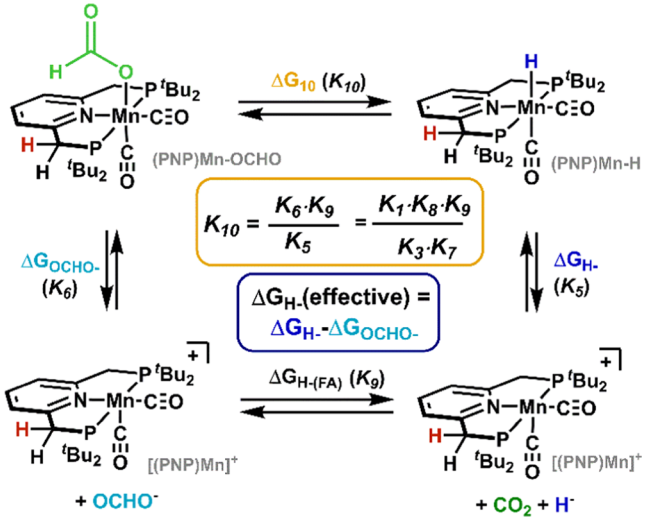

[a]An alternative thermocycle to obtain K_{10} is indicated by the product of equilibrium constants.

Scheme 9. Equilibria Employed to Determine Formate Release[a]

$(PNP)Mn-OCHO \rightleftharpoons ({}^{*}PNP)Mn + FA$	$-\Delta G_{FA} = \sim 4.1$	$(K_3)^{-1}$
$({}^{*}PNP)Mn + H^{+} \rightleftharpoons [(PNP)Mn]^{+}$	$-\Delta G_4 = -25.6$	$(K_4)^{-1}$
$FA \rightleftharpoons H^{+} + OCHO^{-}$	$\Delta G_8 = 28.4$	K_8
$(PNP)Mn-OCHO \rightleftharpoons [(PNP)Mn]^{+} + OCHO^{-}$	$\Delta G_{OCHO-} = \sim 6.9$	K_6

[a]Free energies are in units of kcal·mol^{-1}. The value of ΔG_8 is from ref 14.

CO_2 should be favored by ~5.2 kcal·mol^{-1}. As this reactivity is not observed, it suggests that the barrier for CO_2 insertion is too high. Moreover, that hydride transfer ensues from the Ru analogue that has an effective hydricity of 40.9 kcal·mol^{-1}, reinforces the conclusion that in terms of thermodynamics, CO_2 should insert into **(PNP)Mn−H** to give **(PNP)Mn−OCHO** (Scheme 8, top).

From the equilibria shown in Scheme 8, the free energy associated with CO_2 deinsertion from **(PNP)Mn−(OCHO)** to give **(PNP)Mn−H** under standard conditions is 4.8 kcal·mol^{-1}. This value can be modulated by changing the partial pressure of CO_2. The instability of **(PNP)Mn−(OCHO)** described in Scheme 3 is thus a consequence of the other products that are formed.

The thermochemical analysis provides two key results. First, **(PNP)Mn−H** is not sufficiently hydridic to hydrogenate CO_2 to give $[(PNP)Mn]^{+}$ and $OCHO^{-}$. Subsequent formate binding modulates the effective hydricity to now make it thermodynamically favorable, indicating a kinetic barrier (at room temperature), which is proposed to be overcome under catalytic conditions run at elevated temperatures. This suggests that another hydride may form under catalytic conditions. Second, if **(PNP)Mn−(OCHO)** forms under elevated pressures & temperatures of catalysis, then excess base must drive the loss of formate (see Figure S44)[14,18] at a faster rate than that of **(PNP)Mn−(OCHO)** degradation that gives free ligand. These findings suggest that **(PNP)Mn−(OCHO)** may not be relevant to the catalytic cycle, particularly under mild conditions.

The combined reactivity and thermochemical studies suggest that the two catalytic cycles proposed in Scheme 2 may not be operational. As catalysis occurs in the presence of excess KO^{t}Bu, we hypothesized that under catalytic conditions, both **(PNP)Mn−H** and **(CO_2-PNP)Mn** may give rise to a common anionic hydride intermediate (Scheme 2, right).

Deprotonation of (PNP)Mn−H. Isoelectronic anionic metal hydrides are more hydridic than neutral counterparts, and reduction of a metal hydride to give an anionic congener also increases the hydricity.[49] While there are no examples of the effect that a ligand deprotonation has on the hydricity of complexes that undergo MLC, mechanistic studies by Kempe indicate that a dianionic **Mn−H** is the active catalyst for hydrogenation of imines.[50] Hence, it is expected that an anionic congener of **(PNP)Mn−H** will be more hydridic.

Treatment of **(PNP)Mn−H** with ^{n}BuLi or Schlosser's base results in clean conversion to **[(*PNP)Mn−H]$^{-}$** (only partial conversion is observed with KO^{t}Bu, see Figure S46). The formally 20-electron species is stable as a solid, provided there is no trace moisture in the glovebox atmosphere. Though we have not been able to obtain an X-ray diffraction (XRD) structure, this species has been thoroughly characterized by NMR and IR spectroscopy. Consistent with ligand deprotonation, the ^{31}P NMR spectrum shows an AB pattern with two doublets at 124.6 and 114.9 ppm (J = 56 Hz). The ^{1}H NMR spectrum is diagnostic of dearomatization, with the formally aromatic peaks shifted to 5.23−6.04 ppm. Notably, a hydride resonance that is split into a doublet of doublets is present at −4.57 ppm (J_{HP} = 56, 64 Hz). The anion can be protonated by the addition of a weak acid (HBF_4·$BrC_6H_4P_1$(pyrr)) to quantitatively regenerate **(PNP)Mn−H** (see Figure S60).

The hydricity of **[(*PNP)Mn−H]$^{-}$** is related to the hydricity of neutral **(PNP)Mn−H**, as shown in Scheme 6 and eq 1.

$$\Delta G_{H^-} + 1.364 \cdot pK_a = \Delta G_{H^-(12)} + 1.364 \cdot pK_{a(11)} \quad (1)$$

From Hess's law, knowing the pK_a of **[(*PNP)Mn−H]$^{-}$** allows for determination of it's hydricity, $\Delta G_{H^-(anion)}$.

Titration of **(PNP)Mn−H** with the Wittig base, Ph_3P=CH-(Me)$_2$ (pK_{ip} = 28.7),[51] gave a pK_{ip} value of 31.2 ± 0.2. From eq 1, the hydricity of **[(*PNP)Mn−H]$^{-}$** is found to be 29.5 (±0.4) kcal·mol^{-1}. Hence, deprotonation of the ligand backbone enhances the hydricity by 16.9 kcal·mol^{-1}. The magnitude of this shift is impressive given that the hydricity scale for 1st row transition-metal hydrides in MeCN spans ~40 kcal·mol^{-1}.[49]

Reactivity of [(*PNP)Mn−H]$^{-}$ toward CO_2. It is anticipated that treatment of **[(*PNP)Mn−H]$^{-}$** with CO_2 will result in formate loss via direct hydride transfer, as the hydride transfer is favorable by 15.2 kcal·mol^{-1}. Indeed, the reaction of **[(*PNP)Mn−H]$^{-}$** with 0.85 atm of CO_2 proceeds to produce formate (84% yield), but the product of direct hydride transfer, **(*PNP)Mn**, is not observed (Figure 1, top). Rather, **(CO_2-PNP)Mn** is the major species in solution (~92%), and **(PNP)Mn−H** is also present (~8%). Given the moisture sensitivity of **[(*PNP)Mn−H]$^{-}$**, the neutral hydride is postulated to form from trace moisture.

Monitoring the reaction by ^{31}P NMR spectroscopy indicates that within 3 min of CO_2 addition, **[(*PNP)Mn−H]$^{-}$** is consumed and replaced by two new species that have

https://doi.org/10.1021/acscatal.1c01709
ACS Catal. 2021, 11, 8358−8369

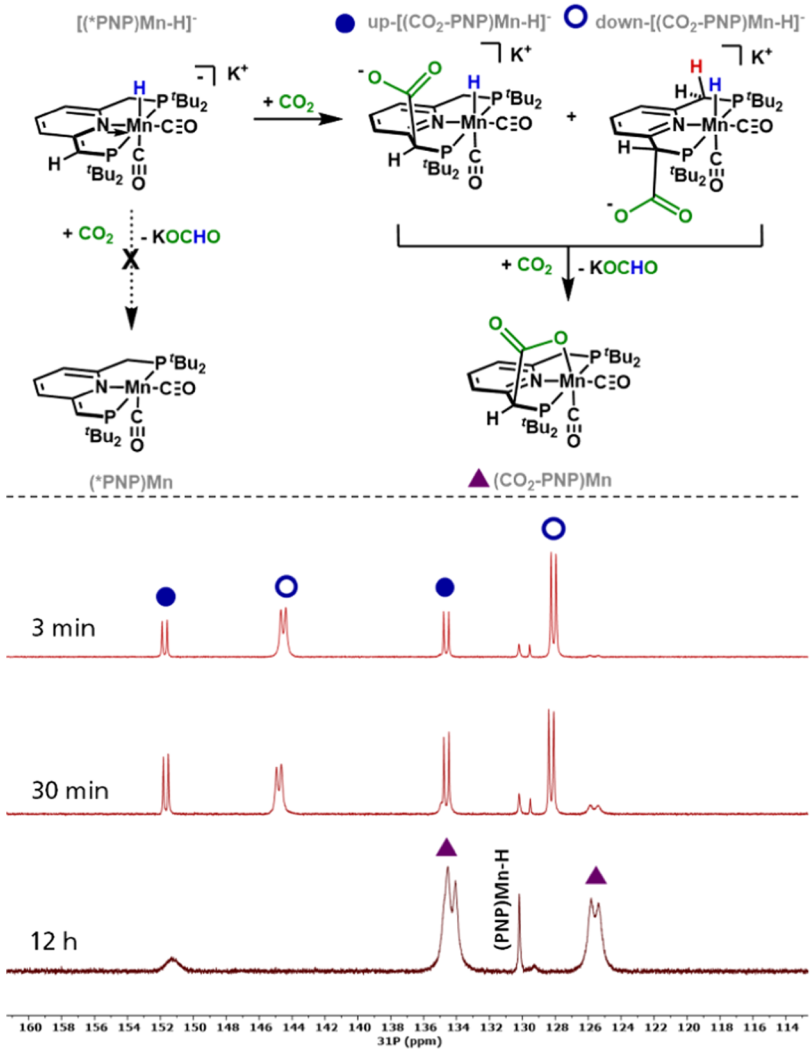

Figure 1. (Top): Observed reactivity of $[(\mathbf{*PNP})\mathbf{Mn{-}H}]^-$ toward CO_2. (Bottom): ^{31}P NMR spectra taken at various times.

inequivalent phosphines (minor: δ = 151.5 & 134.6 ppm, J = 61 Hz; major: δ = 145.2 & 128.5 ppm, J = 59 Hz). Peaks associated with $(\mathbf{CO_2\text{-}PNP})\mathbf{Mn}$ are present at 30 min and continue to grow (as the intermediate peaks decrease) until ~24 h, when the reaction is complete. When the reaction of $[(\mathbf{*PNP})\mathbf{Mn{-}H}]^-$ is repeated with higher CO_2 pressure (~1.5 atm), the reaction is complete within 4 h. Inclusion of H_2 to the reaction does not impact the reaction rate.

Addition of 1 equiv of CO_2 to $[(\mathbf{*PNP})\mathbf{Mn{-}H}]^-$ gives rise to the same two intermediates observed above (Figure S66). Over the course of hours, resonances associated with the kinetic product (major species at 3 min) decrease as it is converted to the thermodynamic product (minor species at 3 min). Of note, the resonances associated with the kinetic product are broadened with fewer CO_2 equiv, consistent with a fluxional process. Two hydride resonances are observed in the ^1H NMR spectrum, with integration that matches that observed in the ^{31}P NMR spectrum. When the reaction is repeated with $^{13}CO_2$, the ^{13}C NMR spectrum shows two resonances at 176.6 and 175.1 ppm, which correspond to ligand-bound CO_2. Taken together, the NMR data suggest that the two intermediates are isomers of $[(\mathbf{CO_2\text{-}PNP})\mathbf{Mn{-}H}]^-$, whereby one has the CO_2 pointing "up" toward the hydride, and the other pointing "down" away from the hydride. DFT-minimized structures of these two isomers in implicit solvent indicate that the up conformer is lower in Gibbs free energy by 0.82 kcal·mol^{-1}. Although this energy gap is likely near the error bars of these DFT computations, the existence of two isomers of nearly equal energy is nonetheless consistent with the experimental observations.

Hence, direct hydride transfer from $[(\mathbf{*PNP})\mathbf{Mn{-}H}]^-$ to CO_2 does not occur. The lack of reactivity is speculated to be due to $[(\mathbf{*PNP})\mathbf{Mn{-}H}]^-$ being a formally 20-electron species. CO_2 insertion that proceeds via an inner-sphere mechanism necessitates transient coordination to the metal;[11] in the absence of hemilabile ligands, this would increase the formal electron count to 22. While an outer-sphere mechanism, whereby the hydride directly attacks CO_2 may be feasible, the observed reactivity indicates that the HOMO of $[(\mathbf{*PNP})\mathbf{Mn{-}H}]^-$ resides primarily on the ligand, consistent with the DFT calculations (Figure S79).

Deprotonation of $(\mathbf{CO_2\text{-}PNP})\mathbf{Mn}$. Given that both $(\mathbf{CO_2\text{-}PNP})\mathbf{Mn}$ and $(\mathbf{PNP})\mathbf{Mn{-}H}$ are precatalysts, if the mechanism proceeds via $[(\mathbf{CO_2\text{-}PNP})\mathbf{Mn{-}H}]^-$, then this species should be accessible starting from $(\mathbf{CO_2\text{-}PNP})\mathbf{Mn}$. Deprotonation of $(\mathbf{CO_2\text{-}PNE})\mathbf{Ru(CO)(H)}$ occurs at the ligand to yield $[(\mathbf{*CO_2\text{-}PNE})\mathbf{Ru(CO)(H)}]^-$.[14,18] Sanford previously observed that introduction of 1 bar of H_2 and CO_2 to $[(\mathbf{*CO_2\text{-}PNN})\mathbf{Ru}$-

https://doi.org/10.1021/acscatal.1c01709
ACS Catal. 2021, 11, 8358−8369

(CO)(H)]$^-$ generates (**CO_2-PNN**)**Ru**(**CO**)(**H**) along with a 15% yield of KOCHO.[18]

Treatment of (**CO_2-PNP**)**Mn** with 1 equiv of KO^{t}Bu generates [(***CO_2-PNP**)**Mn**][**K**]. The ^{31}P NMR spectrum has doublets at 118.7 and 113.7 ppm (J = 104 Hz). Furthermore, the ^{1}H NMR spectrum of (**CO_2-PNP**)**Mn** shows that the aromatic pyridine peaks of the (**CO_2-PNP**)**Mn** shift to 6.21, 5.81, and 5.39 ppm, indicating dearomatization. Single-crystal X-ray diffraction confirmed the dearomatization, with the bond length of the pyridine carbon and the attached methylene spacer decreasing from 1.499 (3) to 1.39 (1)Å (Figure 2). Of

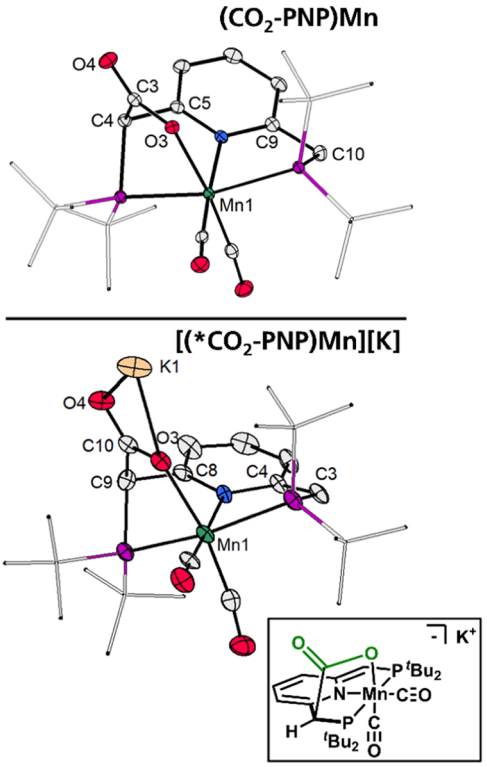

Figure 2. Thermal ellipsoid plots (50%) of (top): (**CO_2-PNP**)**Mn** and (bottom): [(***CO_2-PNP**)**Mn**][**K**]. Hydrogen atoms and solvent molecules are removed for clarity, and only one Mn from the unit cell is shown for the anionic species. Select bond distances (Å) for (**CO_2-PNP**)**Mn**: Mn1−O3: 2.074(2); O3−C3: 1.287(2); C3−O4: 1.227(3); C3−C4: 1.554(3); C4−C5: 1.500(3); and C9−C10: 1.499(3). Select bond distances (Å) for [(***CO_2-PNP**)**Mn**][**K**]: Mn1−O3: 2.099(7); O3−C10: 1.273(2); C10−O4: 1.23(1); C9−C10: 1.53(1); C4−C7: 1.51(1); C3−C4: 1.39(1). Similar bond distances are obtained about Mn2 of the unit cell.

note in the crystal structure of [(***CO_2-PNP**)**Mn**][**K**] is the ∼0.02 Å increase in the Mn−O bond distance relative to (**CO_2-PNP**)**Mn**. Furthermore, the IR stretch associated with the bound CO_2 shifts from 1651 to 1605 cm^{-1} upon deprotonation.

The anion, [(***CO_2-PNP**)**Mn**]$^-$, exists as a potassium-bridged dimer in the solid state. Treatment with 18-crown-6 yields the monomeric potassium adduct, confirmed through single-crystal X-ray diffraction. Attempts to prepare analogous sodium or lithium species were not successful and showed limited stability (see the SI). This suggests that the potassium is essential in stabilizing the anion.

Titration of (**CO_2-PNP**)**Mn** with the Wittig base, $Ph_3P{=}CH(CH_3)_2$ (pK_{ip} = 28.7),[51] yielded a pK_{ip} = 28.7 ± 0.2. This value is more acidic compared to that of (**PNP**)**Mn−H** (pK_{ip} = 31.2).

Reactivity of [(*CO_2-PNP)Mn]$^-$ With H_2. Addition of 0.85 atm of H_2 to [(***CO_2-PNP**)**Mn**]$^-$ results in a color change and precipitation of a colorless solid over 24 h. After heating to 65 °C, NMR spectroscopy indicates that the major Mn species in solution is (**PNP**)**Mn−H**. IR and NMR spectroscopy was used to identify the solid as KOCHO. Quantification of formate by ion chromatography gives 93% yield.

To gain further insight, the reaction was monitored by ^{31}P and ^{1}H NMR spectroscopy (Figure 3). After addition of H_2 to [(***CO_2-PNP**)**Mn**]$^-$, the ^{31}P NMR spectrum shows a pair of doublets that correspond to the thermodynamic isomer of [(**CO_2-PNP**)**Mn−H**]$^-$ described above. Of note, this species remains a minor component of the reaction mixture, with [(***CO_2-PNP**)**Mn**]$^-$ present at all time points; higher H_2 pressures are required to shift the equilibrium (see the SI). Over time, signals associated with this species decay as those for (**PNP**)**Mn−H** grow. The reaction requires heating and days for completion. No other identifiable intermediates are observed.

The conversion of [(***CO_2-PNP**)**Mn**]$^-$ to formate and (**PNP**)**Mn−H** formally requires 2 equiv of H_2. When only 1 equiv of H_2 is added to [(***CO_2-PNP**)**Mn**]$^-$, ∼30% converts to (**PNP**)**Mn−H**.

Proposed Mechanism. We postulate that loss of formate from [(**CO_2-PNP**)**Mn−H**]$^-$ and conversion to (**PNP**)**Mn−H** could occur by 3 different mechanisms. Bimolecular mechanisms, whereby 2 equiv of anionic [(**CO_2-PNP**)**Mn−H**]$^-$ must react with one another, are not considered due to steric and electrostatic arguments. Likewise, a mechanism that proceeds from the neutral (**PNP**)**Mn−OCHO** (gray arrows) is not thought to be operative, at least for low-temperature catalysis (vide infra), given the thermodynamic and mechanistic studies presented above. As catalysis ensues from [(**CO_2-PNP**)**Mn−H**]$^-$, whereby the ligand is deprotonated, revised Noyori-type mechanisms[52,53] (whereby the protonated ligand does not transfer a proton but rather serves as a hydrogen-bond donor) are also not considered.

The first mechanism considered is unimolecular formate loss from [(**CO_2-PNP**)**Mn−H**]$^-$ to give (***PNP**)**Mn**, which then reacts with CO_2 or H_2 to generate (**CO_2-PNP**)**Mn** or (**PNP**)**Mn−H**, respectively (Scheme 10, tan arrows). Given that the reaction of (***PNP**)**Mn** with either gas is complete within minutes and similar thermodynamics associated with the two reactions, if this mechanism is correct then the rate of formate loss should have no dependence on CO_2 or H_2. The data presented are not consistent with this mechanism.

Alternatively, H_2 addition across the C−C bond of [(**CO_2-PNP**)**Mn−H**]$^-$ generates (**PNP**)**Mn−H** and formate in a single step (Scheme 10, blue arrows). If this mechanism is correct, then addition of H_2 to the reaction of [(**CO_2-PNP**)**Mn−H**]$^-$ and CO_2 should be faster (compared to that with no H_2 added). That there is no rate enhancement, and that the reaction of [(***CO_2-PNP**)**Mn**]$^-$ with excess H_2 is significantly slower (and requires heating), suggests that this mechanism is also incorrect.

Finally, the hydride of [(**CO_2-PNP**)**Mn−H**]$^-$ can react with free CO_2 to generate formate and (**CO_2-PNP**)**Mn** (Scheme 10, pink arrow). This is consistent with the observed rate enhancement with more CO_2 pressure. Moreover, the

https://doi.org/10.1021/acscatal.1c01709
ACS Catal. 2021, 11, 8358−8369

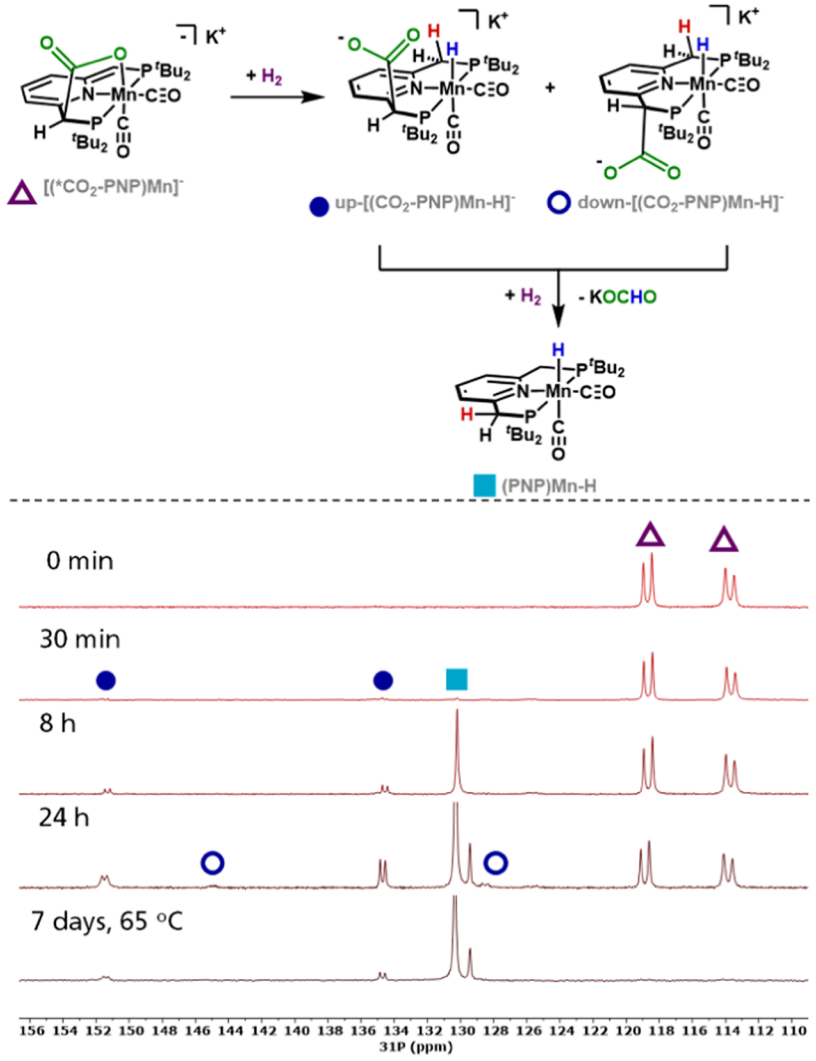

Figure 3. (Top): Observed reactivity of $[(\mathbf{*CO_2\text{-}PNP})\mathbf{Mn}]^-$ with H_2. (Bottom): ^{31}P NMR taken at different time points. The spectrum collected after 7 days was heated at 65 °C for 6 days.

requirement of heat in the reaction of $[(\mathbf{*CO_2\text{-}PNP})\mathbf{Mn{-}H}]^-$ and H_2 suggests that CO_2 may first have to be lost.

Application to Room-Temperature Hydrogenation of CO_2. The use of a first-row transition-metal catalyst for room-temperature hydrogenation of CO_2 is relatively rare.[1,54,55] The stoichiometric reactions described above suggest that room-temperature hydrogenation of CO_2 may be feasible. Addition of CO_2 to $[(\mathbf{*PNP})\mathbf{Mn{-}H}]^-$ readily occurs under ambient conditions (0.85 atm), while addition of H_2 to $[(\mathbf{*CO_2\text{-}PNP})\mathbf{Mn}]^-$ is thermodynamically less favorable (both reactions give $[(\mathbf{CO_2\text{-}PNP})\mathbf{Mn{-}H}]^-$). This difference is due to the difference in pK_a values (see the SI). Given that $[(\mathbf{CO_2\text{-}PNP})\mathbf{Mn{-}H}]^-$ reacts with ambient CO_2 to lose formate to generate $(\mathbf{CO_2\text{-}PNP})\mathbf{Mn}$, it is anticipated that higher H_2 pressures may be required relative to CO_2 to achieve turnover.

Indeed, with 100 equiv of KHMDS, $(\mathbf{PNP})\mathbf{Mn{-}H}$ catalytically hydrogenates CO_2 at room temperature using 2 atm of CO_2 and 15 atm of H_2 (TON = 5) (see SI). While the unoptimized TON is modest, it suggests that knowing the thermodynamic parameters of the system can lead to catalysis under milder conditions. These hydrogenation conditions are similar to those of the stoichiometric studies described (vide supra), indicating that under these mild conditions, the mechanisms shown in the top and bottom of Scheme 2 (and top of Scheme 10) are likely not operative; this may not hold for catalysis under harsher conditions that employ elevated temperatures and higher pressures.

CONCLUSIONS

Herein, we presented the catalytic hydrogenation of CO_2 to formate at a PNP-ligated Mn catalyst. Both reactivity studies and thermochemical analysis indicate that the traditional mechanism, whereby CO_2 inserts into $(\mathbf{PNP})\mathbf{Mn{-}H}$, is not likely to occur (Scheme 10, gray arrows). When formate binding is considered, the effective hydricity of the catalyst is sufficient to reduce CO_2, yet this reactivity is not observed. This contrasts with studies on the Ru analogue.[14,18] These results underscore how subtle changes in the catalyst can alter the reactivity.

Additionally, it was found that deprotonation of the ligand backbone of $(\mathbf{PNP})\mathbf{Mn{-}H}$ generates $[(\mathbf{*PNP})\mathbf{Mn{-}H}]^-$, which is more hydridic by 16.9 kcal·mol^{-1}. This appears to be an underexplored design strategy and may be pertinent to many published hydrogenation reactions. Notably, mechanistic work by Kempe indicates that the reactive hydride is dianionic in a related system that can undergo MLC.[50] Bergens showed

https://doi.org/10.1021/acscatal.1c01709
ACS Catal. 2021, 11, 8358−8369

Scheme 10. Possible Mechanisms for CO_2 Hydrogenation to Formate[a]

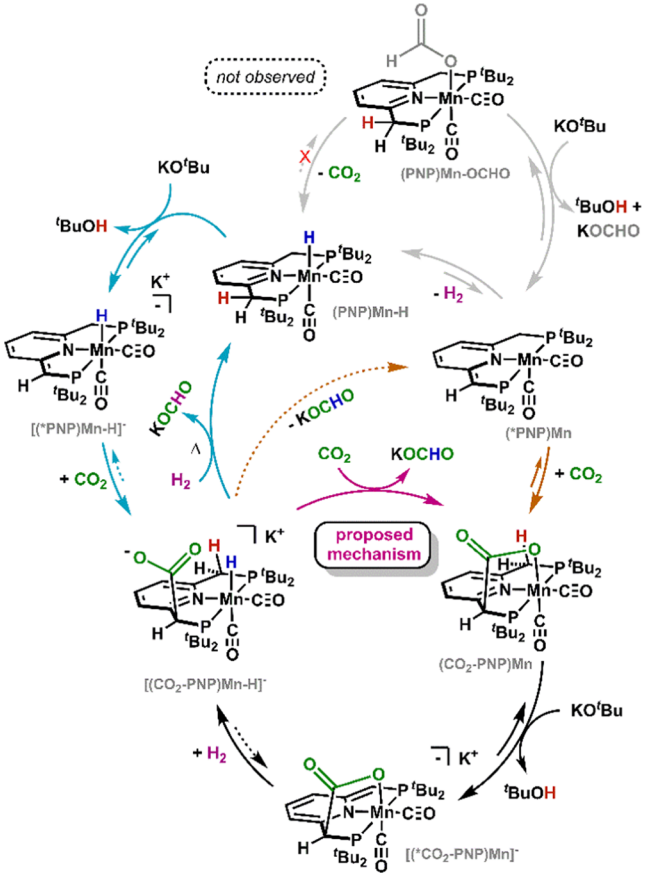

[a]All reactions/equilibria with solid arrows have been observed, and those with dashed lines are included for completeness. The mechanism shown at the bottom is consistent with all experimental data.

that hydride transfer to amides and imines at a Noyori-type Ru catalyst occurs after deprotonation of the ligand (to give an anionic catalyst);[56] it was found that catalytic amounts of the base were required as the conjugate acid, which then protonated the substrate. Given that most catalytic transformations mediated by catalysts capable of undergoing MLC occur in the presence of catalytic amounts of the base,[57−59] it is conceivable that hydride transfer occurs from an anionic deprotonated species.

Despite now having sufficient thermodynamic driving force to hydrogenate CO_2 (in the absence of formate binding to the Mn), no formate is directly produced from $[(\mathbf{*PNP})\mathbf{Mn{-}H}]^-$. Rather, CO_2 coordinates the backbone, and formate is lost from $[(\mathbf{CO_2\text{-}PNP})\mathbf{Mn{-}H}]^-$. It is speculated that the lack of CO_2 insertion is due to the high-electron count about the Mn, with the reactivity occurring at the ligand instead of at the Mn. These findings reinforce the importance of considering relative kinetic barriers and just not only the thermodynamic parameters in predicting reactivity.

The mechanism that is most consistent with the experimental data proceeds via a catalytic cycle that necessitates a ligand-bound CO_2 (Scheme 10, bottom). While such species have been invoked as detrimental,[25,40] both thermochemical and reactivity studies suggest that it is required for the hydrogenation of CO_2. Now, anionic hydride $[(\mathbf{CO_2\text{-}PNP})\mathbf{Mn{-}H}]^-$ can be accessed and is sufficiently hydridic to reduce CO_2. This intermediate is 18-electron and lacks an electrophilic site on the ligand, allowing for hydride transfer to occur. While the hydricity of this species cannot be measured due to its inherent instability, addition of the negative charge increases the hydricity. Given that other carbonyl substrates bind MLC catalysts analogously, mechanisms that proceed with the "bound" substrate should be considered, particularly when the equilibrium toward H_2 rivals that toward the substrate (CO_2, in this case). We emphasize that this mechanism may not be dominant under harsher conditions (increased pressure and temperature), and that it may not hold for other MLC catalysts, particularly those that undergo deprotonation at an amine.[52,53] Nonetheless, analogous mechanisms should be considered in mechanistic schemes, particularly those where deprotonation occurs at a nonpolar C−H bond.

Overall, this work is pertinent to advancing mechanistic schemes and catalyst design strategies for (de)hydrogenation catalysts. The results emphasize that caution must be taken in considering mechanisms, particularly in systems that are capable of undergoing MLC; substrate binding to the backbone and hydride transfer from a deprotonated species were identified in the system investigated. Consideration of such deviations from established mechanistic hypotheses should be considered more broadly. This is particularly true for CO_2 hydrogenations at catalysts capable of undergoing MLC, which are run under basic conditions.

■ ASSOCIATED CONTENT

Supporting Information

The Supporting Information is available free of charge at https://pubs.acs.org/doi/10.1021/acscatal.1c01709.

All experimental details, including syntheses, spectroscopic data, equilibrium plots (PDF)

Crystallographic data (CIF)

■ AUTHOR INFORMATION

Corresponding Author

Caroline T. Saouma − *Department of Chemistry, University of Utah, Salt Lake City, Utah 84112, United States;* orcid.org/0000-0003-1170-6175; Email: caroline.saouma@utah.edu

Authors

Kevin Schlenker − *Department of Chemistry, University of Utah, Salt Lake City, Utah 84112, United States*

Elizabeth G. Christensen − *Department of Chemistry, University of Utah, Salt Lake City, Utah 84112, United States*

Asylbek A. Zhanserkeev − *Department of Chemistry, University of Utah, Salt Lake City, Utah 84112, United States*

Gabriel R. McDonald − *Department of Chemistry, University of Utah, Salt Lake City, Utah 84112, United States*

Emily L. Yang − *Department of Chemistry, University of Utah, Salt Lake City, Utah 84112, United States*

Kevin T. Lutz − *Department of Chemistry, University of Utah, Salt Lake City, Utah 84112, United States*

Ryan P. Steele − *Department of Chemistry, University of Utah, Salt Lake City, Utah 84112, United States;* orcid.org/0000-0002-3292-9805

https://doi.org/10.1021/acscatal.1c01709
ACS Catal. 2021, 11, 8358−8369

Ryan T. VanderLinden − *Department of Chemistry, University of Utah, Salt Lake City, Utah 84112, United States;* orcid.org/0000-0002-0128-1284

Complete contact information is available at: https://pubs.acs.org/10.1021/acscatal.1c01709

Author Contributions

The manuscript was written through contributions of all authors. All authors have given approval to the final version of the manuscript.

Funding

The authors gratefully acknowledge start-up funding from the University of Utah & USTAR and NSF CAREER (1945646). The NMR results included in this report were recorded at the David M. Grant NMR Center, a University of Utah Core Facility. Funds for construction of the Center and the helium recovery system were obtained from the University of Utah and the National Institutes of Health awards 1C06RR017539-01A1 and 3R01GM063540-17W1, respectively. NMR instruments were purchased with the support of the University of Utah and the National Institutes of Health award 1S10OD25241-01.

Notes

The authors declare no competing financial interest.

■ ACKNOWLEDGMENTS

We thank Dr. Peter Flynn for the help with NMR experiments. Royce Song, Maxwell Reese, and Mallory Philliber helped obtain preliminary hydrogenation data.

■ REFERENCES

(1) Wang, W. H.; Himeda, Y.; Muckerman, J. T.; Manbeck, G. F.; Fujita, E. CO_2 Hydrogenation to Formate and Methanol as an Alternative to Photo- and Electrochemical CO_2 Reduction. *Chem. Rev.* **2015**, *115*, 12936−12973.

(2) Burkart, M. D.; Hazari, N.; Tway, C. L.; Zeitler, E. L. Opportunities and Challenges for Catalysis in Carbon Dioxide Utilization. *ACS Catal.* **2019**, *9*, 7937−7956.

(3) Hepburn, C.; Adlen, E.; Beddington, J.; Carter, E. A.; Fuss, S.; Mac Dowell, N.; Minx, J. C.; Smith, P.; Williams, C. K. The technological and economic prospects for CO_2 utilization and removal. *Nature* **2019**, *575*, 87−97.

(4) Artz, J.; Müller, T. E.; Thenert, K.; Kleinekorte, J.; Meys, R.; Sternberg, A.; Bardow, A.; Leitner, W. Sustainable Conversion of Carbon Dioxide: An Integrated Review of Catalysis and Life Cycle Assessment. *Chem. Rev.* **2018**, *118*, 434−504.

(5) Yu, X.; Pickup, P. G. Recent advances in direct formic acid fuel cells (DFAFC). *J. Power Sources* **2008**, *182*, 124−132.

(6) Grasemann, M.; Laurenczy, G. Formic acid as a hydrogen source − recent developments and future trends. *Energy Environ. Sci.* **2012**, *5*, 8171−8181.

(7) Schmeier, T. J.; Dobereiner, G. E.; Crabtree, R. H.; Hazari, N. Secondary Coordination Sphere Interactions Facilitate the Insertion Step in an Iridium(III) CO_2 Reduction Catalyst. *J. Am. Chem. Soc.* **2011**, *133*, 9274−9277.

(8) Ziebart, C.; Federsel, C.; Anbarasan, P.; Jackstell, R.; Baumann, W.; Spannenberg, A.; Beller, M. Well-Defined Iron Catalyst for Improved Hydrogenation of Carbon Dioxide and Bicarbonate. *J. Am. Chem. Soc.* **2012**, *134*, 20701−20704.

(9) Wesselbaum, S.; Moha, V.; Meuresch, M.; Brosinski, S.; Thenert, K. M.; Kothe, J.; Stein, T. V.; Englert, U.; Hölscher, M.; Klankermayer, J.; Leitner, W. Hydrogenation of carbon dioxide to methanol using a homogeneous ruthenium-Triphos catalyst: from mechanistic investigations to multiphase catalysis. *Chem. Sci.* **2015**, *6*, 693−704.

(10) Waldie, K. M.; Ostericher, A. L.; Reineke, M. H.; Sasayama, A. F.; Kubiak, C. P. Hydricity of Transition-Metal Hydrides: Thermodynamic Considerations for CO_2 Reduction. *ACS Catal.* **2018**, *8*, 1313−1324.

(11) Heimann, J. E.; Bernskoetter, W. H.; Hazari, N.; Mayer, J. M. Acceleration of CO_2 insertion into metal hydrides: ligand, Lewis acid, and solvent effects on reaction kinetics. *Chem. Sci.* **2018**, *9*, 6629−6638.

(12) Heimann, J. E.; Bernskoetter, W. H.; Hazari, N. Understanding the Individual and Combined Effects of Solvent and Lewis Acid on CO_2 Insertion into a Metal Hydride. *J. Am. Chem. Soc.* **2019**, *141*, 10520−10529.

(13) Ceballos, B. M.; Yang, J. Y. Directing the reactivity of metal hydrides for selective CO_2 reduction. *Proc. Natl. Acad. Sci. U.S.A.* **2018**, *115*, 12686−12691.

(14) Mathis, C. L.; Geary, J.; Ardon, Y.; Reese, M. S.; Philliber, M. A.; VanderLinden, R. T.; Saouma, C. T. Thermodynamic Analysis of Metal-Ligand Cooperativity of PNP Ru Complexes: Implications for CO_2 Hydrogenation to Methanol and Catalyst Inhibition. *J. Am. Chem. Soc.* **2019**, *141*, 14317−14328.

(15) Taheri, A.; Thompson, E. J.; Fettinger, J. C.; Berben, L. A. An Iron Electrocatalyst for Selective Reduction of CO_2 to Formate in Water: Including Thermochemical Insights. *ACS Catal.* **2015**, *5*, 7140−7151.

(16) Bhattacharya, M.; Sebghati, S.; VanderLinden, R. T.; Saouma, C. T. Toward Combined Carbon Capture and Recycling: Addition of an Amine Alters the Product Selectivity from CO to Formic Acid in Manganese Catalyzed Reduction of CO_2. *J. Am. Chem. Soc.* **2020**, *142*, 17589−17597.

(17) Hu, J.; Bruch, Q. J.; Miller, A. J. M. Temperature and Solvent Effects on H_2 Splitting and Hydricity: Ramifications on CO_2 Hydrogenation by a Rhenium Pincer Catalyst. *J. Am. Chem. Soc.* **2021**, *143*, 945−954.

(18) Huff, C. A.; Sanford, M. S. Catalytic CO_2 Hydrogenation to Formate by a Ruthenium Pincer Complex. *ACS Catal.* **2013**, *3*, 2412−2416.

(19) Kothandaraman, J.; Goeppert, A.; Czaun, M.; Olah, G. A.; Prakash, G. K. S. Conversion of CO_2 from Air into Methanol Using a Polyamine and a Homogeneous Ruthenium Catalyst. *J. Am. Chem. Soc.* **2016**, *138*, 778−781.

(20) Filonenko, G. A.; van Putten, R.; Schulpen, E. N.; Hensen, E. J. M.; Pidko, E. A. Highly Efficient Reversible Hydrogenation of Carbon Dioxide to Formates Using a Ruthenium PNP-Pincer Catalyst. *ChemCatChem* **2014**, *6*, 1485.

(21) Daw, P.; Chakraborty, S.; Leitus, G.; Diskin-Posner, Y.; Ben-David, Y.; Milstein, D. Selective N-Formylation of Amines with H_2 and CO_2 Catalyzed by Cobalt Pincer Complexes. *ACS Catal.* **2017**, *7*, 2500−2504.

(22) Scheuermann, M. L.; Semproni, S. P.; Pappas, I.; Chirik, P. J. Carbon Dioxide Hydrosilylation Promoted by Cobalt Pincer Complexes. *Inorg. Chem.* **2014**, *53*, 9463−9465.

(23) Langer, R.; Diskin-Posner, Y.; Leitus, G.; Shimon, L. J. W.; Ben-David, Y.; Milstein, D. Low-Pressure Hydrogenation of Carbon Dioxide Catalyzed by an Iron Pincer Complex Exhibiting Noble Metal Activity. *Angew. Chem., Int. Ed.* **2011**, *50*, 9948−9952.

(24) Zhang, Y.; MacIntosh, A. D.; Wong, J. L.; Bielinski, E. A.; Williard, P. G.; Mercado, B. Q.; Hazari, N.; Bernskoetter, W. H. Iron catalyzed CO_2 hydrogenation to formate enhanced by Lewis acid co-catalysts. *Chem. Sci.* **2015**, *6*, 4291−4299.

(25) Rivada-Wheelaghan, O.; Dauth, A.; Leitus, G.; Diskin-Posner, Y.; Milstein, D. Synthesis and Reactivity of Iron Complexes with a New Pyrazine-Based Pincer Ligand, and Application in Catalytic Low-Pressure Hydrogenation of Carbon Dioxide. *Inorg. Chem.* **2015**, *54*, 4526−4538.

(26) Kar, S.; Goeppert, A.; Kothandaraman, J.; Prakash, G. K. S. Manganese-Catalyzed Sequential Hydrogenation of CO_2 to Methanol via Formamide. *ACS Catal.* **2017**, *7*, 6347−6351.

(27) Kumar, A.; Daw, P.; Espinosa-Jalapa, N. A.; Leitus, G.; Shimon, L. J. W.; Ben-David, Y.; Milstein, D. CO_2 activation by manganese

pincer complexes through different modes of metal-ligand cooperation. *Dalton Trans.* **2019**, *48*, 14580−14584.
(28) Rezayee, N. M.; Huff, C. A.; Sanford, M. S. Tandem Amine and Ruthenium-Catalyzed Hydrogenation of CO_2 to Methanol. *J. Am. Chem. Soc.* **2015**, *137*, 1028−1031.
(29) Khusnutdinova, J. R.; Garg, J. A.; Milstein, D. Combining Low-Pressure CO_2 Capture and Hydrogenation To Form Methanol. *ACS Catal.* **2015**, *5*, 2416−2422.
(30) Filonenko, G. A.; Conley, M. P.; Copéret, C.; Lutz, M.; Hensen, E. J. M.; Pidko, E. A. The impact of Metal−Ligand Cooperation in Hydrogenation of Carbon Dioxide Catalyzed by Ruthenium PNP Pincer. *ACS Catal.* **2013**, *3*, 2522−2526.
(31) Filonenko, G. A.; Smykowski, D.; Szyja, B. M.; Li, G.; Szczygieł, J.; Hensen, E. J. M.; Pidko, E. A. Catalytic Hydrogenation of CO_2 to Formates by a Lutidine-Derived Ru−CNC Pincer Complex: Theoretical Insight into the Unrealized Potential. *ACS Catal.* **2015**, *5*, 1145−1154.
(32) Vogt, M.; Gargir, M.; Iron, M. A.; Diskin-Posner, Y.; Ben-David, Y.; Milstein, D. A new mode of activation of CO_2 by metal-ligand cooperation with reversible C-C and M-O bond formation at ambient temperature. *Chem. - Eur. J.* **2012**, *18*, 9194−9197.
(33) Johnson, M. C.; Rogers, D.; Kaminsky, W.; Cossairt, B. M. CO_2 Hydrogenation Catalyzed by a Ruthenium Protic N-Heterocyclic Carbene Complex. *Inorg. Chem.* **2021**, *60*, 5996−6003.
(34) Feller, M.; Gellrich, U.; Anaby, A.; Diskin-Posner, Y.; Milstein, D. Reductive Cleavage of CO_2 by Metal−Ligand-Cooperation Mediated by an Iridium Pincer Complex. *J. Am. Chem. Soc.* **2016**, *138*, 6445−6454.
(35) Vogt, M.; Nerush, A.; Diskin-Posner, Y.; Ben-David, Y.; Milstein, D. Reversible CO_2 binding triggered by metal−ligand cooperation in a rhenium(I) PNP pincer-type complex and the reaction with dihydrogen. *Chem. Sci.* **2014**, *5*, 2043−2051.
(36) Vogt, M.; Rivada-Wheelaghan, O.; Iron, M. A.; Leitus, G.; Diskin-Posner, Y.; Shimon, L. J. W.; Ben-David, Y.; Milstein, D. Anionic Nickel(II) Complexes with Doubly Deprotonated PNP Pincer-Type Ligands and Their Reactivity toward CO_2. *Organometallics* **2013**, *32*, 300−308.
(37) Huff, C. A.; Kampf, J. W.; Sanford, M. S. Reversible carbon−carbon bond formation between carbonyl compounds and a ruthenium pincer complex. *Chem. Commun.* **2013**, *49*, 7147−7149.
(38) Mukherjee, A.; Nerush, A.; Leitus, G.; Shimon, L. J. W.; Ben David, Y.; Espinosa Jalapa, N. A.; Milstein, D. Manganese-Catalyzed Environmentally Benign Dehydrogenative Coupling of Alcohols and Amines to Form Aldimines and H_2: A Catalytic and Mechanistic Study. *J. Am. Chem. Soc.* **2016**, *138*, 4298−4301.
(39) Montag, M.; Zhang, J.; Milstein, D. Aldehyde Binding through Reversible C−C Coupling with the Pincer Ligand upon Alcohol Dehydrogenation by a PNP−Ruthenium Catalyst. *J. Am. Chem. Soc.* **2012**, *134*, 10325−10328.
(40) Filonenko, G. A.; Hensen, E. J. M.; Pidko, E. A. Mechanism of CO_2 hydrogenation to formates by homogeneous Ru-PNP pincer catalyst: from a theoretical description to performance optimization. *Catal. Sci. Technol.* **2014**, *4*, 3474−3485.
(41) Bertini, F.; Glatz, M.; Gorgas, N.; Stoger, B.; Peruzzini, M.; Veiros, L. F.; Kirchner, K.; Gonsalvi, L. Carbon dioxide hydrogenation catalysed by well-defined Mn(I) PNP pincer hydride complexes. *Chem. Sci.* **2017**, *8*, 5024−5029.
(42) Rønne, M. H.; Cho, D.; Madsen, M. R.; Jakobsen, J. B.; Eom, S.; Escoudé, É.; Hammershøj, H. C. D.; Nielsen, D. U.; Pedersen, S. U.; Baik, M.-H.; Skrydstrup, T.; Daasbjerg, K. Ligand-Controlled Product Selectivity in Electrochemical Carbon Dioxide Reduction Using Manganese Bipyridine Catalysts. *J. Am. Chem. Soc.* **2020**, *142*, 4265−4275.
(43) Léval, A.; Agapova, A.; Steinlechner, C.; Alberico, E.; Junge, H.; Beller, M. Hydrogen production from formic acid catalyzed by a phosphine free manganese complex: investigation and mechanistic insights. *Green Chem.* **2020**, *22*, 913−920.
(44) Tondreau, A. M.; Boncella, J. M. 1,2-Addition of Formic or Oxalic Acid to $^{-}N\{CH_2CH_2(PiPr_2)\}_2$-Supported Mn(I) Dicarbonyl Complexes and the Manganese-Mediated Decomposition of Formic Acid. *Organometallics* **2016**, *35*, 2049−2052.
(45) Atmospheric pressure in Salt Lake City, Utah, is ∼ 0.85 atm.
(46) Brereton, K. R.; Jadrich, C. N.; Stratakes, B. M.; Miller, A. J. M. Thermodynamic Hydricity across Solvents: Subtle Electronic Effects and Striking Ligation Effects in Iridium Hydrides. *Organometallics* **2019**, *38*, 3104−3110.
(47) Kaljurand, I.; Saame, J.; Rodima, T.; Koppel, I.; Koppel, I. A.; Kogel, J. F.; Sundermeyer, J.; Kohn, U.; Coles, M. P.; Leito, I. Experimental Basicities of Phosphazene, Guanidinophosphazene, and Proton Sponge Superbases in the Gas Phase and Solution. *J. Phys. Chem. A* **2016**, *120*, 2591−2604.
(48) Pitman, C. L.; Brereton, K. R.; Miller, A. J. M. Aqueous Hydricity of Late Metal Catalysts as a Continuum Tuned by Ligands and the Medium. *J. Am. Chem. Soc.* **2016**, *138*, 2252−2260.
(49) Wiedner, E. S.; Chambers, M. B.; Pitman, C. L.; Bullock, R. M.; Miller, A. J. M.; Appel, A. M. Thermodynamic Hydricity of Transition Metal Hydrides. *Chem. Rev.* **2016**, *116*, 8655−8692.
(50) Freitag, F.; Irrgang, T.; Kempe, R. Mechanistic Studies of Hydride Transfer to Imines from a Highly Active and Chemoselective Manganate Catalyst. *J. Am. Chem. Soc.* **2019**, *141*, 11677−11685.
(51) Saame, J.; Rodima, T.; Tshepelevitsh, S.; Kutt, A.; Kaljurand, I.; Haljasorg, T.; Koppel, I. A.; Leito, I. Experimental Basicities of Superbasic Phosphonium Ylides and Phosphazenes. *J. Org. Chem.* **2016**, *81*, 7349−7361.
(52) Mandal, S. C.; Rawat, K. S.; Pathak, B. A computational study on ligand assisted vs. ligand participation mechanisms for CO_2 hydrogenation: importance of bifunctional ligand based catalysts. *Phys. Chem. Chem. Phys.* **2019**, *21*, 3932−3941.
(53) Dub, P. A.; Gordon, J. C. The role of the metal-bound N−H functionality in Noyori-type molecular catalysts. *Nat. Rev. Chem.* **2018**, *2*, 396−408.
(54) Vollmer, M. V.; Ye, J.; Linehan, J. C.; Graziano, B. J.; Preston, A.; Wiedner, E. S.; Lu, C. C. Cobalt-Group 13 Complexes Catalyze CO_2 Hydrogenation via a Co(−I)/Co(I) Redox Cycle. *ACS Catal.* **2020**, *10*, 2459−2470.
(55) Jeletic, M. S.; Mock, M. T.; Appel, A. M.; Linehan, J. C. A. Cobalt-Based Catalyst for the Hydrogenation of CO_2 under Ambient Conditions. *J. Am. Chem. Soc.* **2013**, *135*, 11533−11536.
(56) John, J. M.; Takebayashi, S.; Dabral, N.; Miskolzie, M.; Bergens, S. H. Base-Catalyzed Bifunctional Addition to Amides and Imides at Low Temperature. A New Pathway for Carbonyl Hydrogenation. *J. Am. Chem. Soc.* **2013**, *135*, 8578−8584.
(57) Alig, L.; Fritz, M.; Schneider, S. First-Row Transition Metal (De)Hydrogenation Catalysis Based On Functional Pincer Ligands. *Chem. Rev.* **2019**, *119*, 2681−2751.
(58) Gunanathan, C.; Milstein, D. Bond Activation and Catalysis by Ruthenium Pincer Complexes. *Chem. Rev.* **2014**, *114*, 12024−12087.
(59) Khusnutdinova, J. R.; Milstein, D. Metal−Ligand Cooperation. *Angew. Chem., Int. Ed.* **2015**, *54*, 12236−12273.

https://doi.org/10.1021/acscatal.1c01709
ACS Catal. 2021, 11, 8358−8369